The Astrophysical Journal Letters, 714:L190–L195, 2010 May 10 doi:10.1088/2041-8205/714/2/L190

NO EVOLUTION IN THE IR–RADIO RELATION FOR IR-LUMINOUS GALAXIES AT $z < 2$ IN THE COSMOS FIELD*

M. T. Sargent[1], E. Schinnerer[1], E. Murphy[2], C. L. Carilli[3], G. Helou[4], H. Aussel[5], E. Le Floc'h[5], D. T. Frayer[6], O. Ilbert[7], P. Oesch[8], M. Salvato[9], V. Smolčić[10], J. Kartaltepe[11], and D. B. Sanders[12]
[1] Max-Planck-Institut für Astronomie, Königstuhl 17, D-69117 Heidelberg, Germany; markmr@mpia.de
[2] *Spitzer* Science Center, MC 314-6, California Institute of Technology, Pasadena, CA 91125, USA
[3] National Radio Astronomy Observatory, P.O. Box 0, Socorro, NM 87801-0387, USA
[4] Infrared Processing and Analysis Center, MC 100-22, California Institute of Technology, Pasadena, CA 91125, USA
[5] AIM Unité Mixte de Recherche CEA CNRS Université Paris VII UMR n158, France
[6] National Radio Astronomy Observatory, P.O. Box 2, Green Bank, WV 24944, USA
[7] Laboratoire d'Astrophysique de Marseille, Université de Provence, CNRS, 38 rue Frédéric Joliot-Curie, F-13388 Marseille Cedex 13, France
[8] Department of Physics, ETH Zurich, CH-8093 Zurich, Switzerland
[9] Max-Planck-Institut für Plasmaphysik, Boltzmanstrasse, D-85741 Garching, Germany
[10] California Institute of Technology, MC 105-24, 1200 East California Boulevard, Pasadena, CA 91125, USA
[11] National Optical Astronomy Observatory, 950 North Cherry Avenue, Tucson, AZ 85726, USA
[12] Institute for Astronomy, 2680 Woodlawn Drive, University of Hawaii, Honolulu, HI 96822, USA
Received 2010 January 12; accepted 2010 March 22; published 2010 April 12

ABSTRACT

Previous observational studies of the infrared (IR)–radio relation out to high redshift employed any detectable star-forming systems at a given redshift within the restricted area of cosmological survey fields. Consequently, the evolution inferred relies on a comparison between the average IR/radio properties of (1) very IR-luminous high-z sources and (2) more heterogeneous low(er)-z samples that often lack the strongest IR emitters. In this Letter, we consider populations of objects with comparable luminosities over the last 10 Gyr by taking advantage of deep IR (especially *Spitzer* 24 μm) and Very Large Array 1.4 GHz observations of the COSMOS field. Consistent with recent model predictions, both Ultra Luminous Infrared Galaxies and galaxies on the bright end of the evolving IR luminosity function do not display any change in their average IR/radio ratios out to $z \sim 2$ when corrected for bias. Uncorrected data suggested ∼0.3 dex of positive evolution.

Key words: cosmology: observations – galaxies: active – galaxies: evolution – infrared: galaxies – radio continuum: galaxies – surveys

1. INTRODUCTION

The infrared (IR)/radio properties of galaxies at successively higher redshift have been probed in the past decade using either statistical samples from cosmological survey fields (e.g., Appleton et al. 2004; Frayer et al. 2006; Sargent et al. 2010, hereafter: S10), the stacking technique (e.g., Carilli et al. 2008; Ivison et al. 2010), or dedicated samples of specific objects (e.g., submillimeter galaxies (SMGs); Kovács et al. 2006; Hainline et al. 2009; Michałowski et al. 2010). Evolutionary studies, all based on samples poorly matched in terms of bolometric luminosity at low and high redshift, have provided conflicting results, concluding that the local IR–radio relation either does (e.g., Garrett 2002; Appleton et al. 2004; Ibar et al. 2008; Garn et al. 2009; S10) or does not (e.g., Seymour et al. 2009; Ivison et al. 2010) hold out to high redshift.

Recently, predictions have been made for the redshift evolution of the IR/radio properties of star-forming (SF) galaxies having different luminosities and geometries (e.g., compact starbursts and normal SF disks; Murphy 2009; Lacki & Thompson 2010). The current generation of IR and radio observatories can directly detect the brightest of these systems over a significant fraction of Hubble time, provided that sufficiently large cosmological volumes are sampled. Here, we make use of the Very Large Array (VLA) and *Spitzer* coverage of the 2 deg^2 COSMOS field to construct (see Section 2) a volume-limited sample of Ultra Luminous Infrared Galaxies (ULIRGs) at $z < 2$ that allows a direct comparison of observations and theory. Our findings are presented in Section 3 and discussed in Section 4.

We adopt the *WMAP*-5 cosmology ($\Omega_m = 0.258$, $\Omega_\Lambda + \Omega_m = 1$, and $H_0 = 71.9$ km s^{-1} Mpc^{-1}; Dunkley et al. 2009).

2. DATA AND SAMPLE SELECTION

2.1. IR and Radio Measurements

The 1.4 GHz map (Schinnerer et al. 2007) of the 2 deg^2 COSMOS field reaches an average sensitivity of ∼0.017 mJy beam^{-1} (FWHM = 2.″5). Here, we use the VLA-COSMOS "Joint" Catalog (Schinnerer et al. 2010) containing ∼2900 sources detected with signal-to-noise ratio, S/N $\geqslant$ 5. *Spitzer*/MIPS imaging by the S-COSMOS project (Sanders et al. 2007) achieves a resolution of 5.″8 (18.″6) and a 1σ point source detection limit of ∼0.018 (1.7) mJy at 24 (70) μm (for details see Le Floc'h et al. 2009 and Frayer et al. 2009). The depth of the 24 μm observations exceeds that at 70 μm and 1.4 GHz by roughly a factor of 7 in terms of equivalent IR luminosity (see Figure 1 in S10). At an equal detection significance level (3σ), the 24 μm catalog consequently is roughly 20-fold larger than the 70 μm source list (∼50,000 versus 2700). *Spitzer* detections were matched to the VLA-COSMOS sources using a search radius of FWHM/3 for either IR filter. Ambiguous radio-IR associations were removed from the sample. Since the 1.4 GHz catalog is restricted to sources with S/N $\geqslant$ 5, we re-analyzed the radio map at the position of unmatched IR sources

* Partly based on observations collected at the European Organization for Astronomical Research in the Southern Hemisphere, Chile, ESO program ID 175.A-0839.

and added all resulting detections with S/N > 3 (∼2100 objects) to the sample. For more information on the band-merging and the flux distributions of the (matched and unmatched) IR and radio sources, we refer to the detailed description in S10.

We use the joint flux information at 24 and 70 μm to determine—given the known redshift (see Section 2.2)—the best-fitting synthetic IR spectral energy distribution (SED) and thence the IR luminosity, $L_{\rm TIR} \equiv L(8\text{–}1000\,\mu{\rm m})$. As described in Section 4 of S10 (see also Murphy et al. 2009, for additional details on the SED fitting), templates according to Chary & Elbaz (2001) are used for galaxies directly detected in both MIPS filters. For sources only detected at 24 μm, we also fit the *Spitzer* photometry (including the 70 μm upper flux limit) with Dale & Helou (2002) template SEDs and define the best estimate of the IR luminosity as the average $L_{\rm TIR}$ from the two separate fits. Inferring $L_{\rm TIR}$ from only two bands at wavelengths shorter than the peak of the IR emission is expected to lead to uncertainties of a factor of 2–5 (Murphy et al. 2009; Kartaltepe et al. 2010). Although our estimates of $L_{\rm TIR}$ are thus less precise than those presented by, e.g., Ivison et al. (2010) for a similar study, there is no consensus in the literature that they are systematically biased to low or high fluxes (see the discussion in S10, Section 6.5).

The IR/radio properties of our sources are characterized by the logarithmic total IR (TIR)/radio flux ratio $q_{\rm TIR}$ (Helou et al. 1985):

$$q_{\rm TIR} = \log\left(\frac{L_{\rm TIR}}{3.75\times10^{12}\,{\rm W}}\right) - \log\left(\frac{L_{1.4\,{\rm GHz}}}{{\rm W\,Hz^{-1}}}\right). \quad (1)$$

The rest-frame 1.4 GHz luminosity $L_{1.4\,{\rm GHz}}$ is

$$L_{1.4\,{\rm GHz}}[{\rm W\,Hz^{-1}}] = \frac{4\pi\,D_L(z)^2}{(1+z)^{1-\alpha}}\,S_\nu(1.4\,{\rm GHz}), \quad (2)$$

where $S_\nu(1.4\,{\rm GHz})$ is the observed integrated radio flux density of the source and $D_L(z)$ is the luminosity distance. The K-correction $(1+z)^{-(1-\alpha)}$ depends on the spectral index of the synchrotron emission, which is set to $\alpha = 0.8$ (Condon 1992). Given the mean spectral slopes typically measured for faint extragalactic radio sources ($0.4 \lesssim \alpha \lesssim 0.9$; e.g., Ibar et al. 2009) our values of $L_{1.4\,{\rm GHz}}$ should be accurate to within 40 (70)% at $z \sim 1$ (2). The main contribution to uncertainties on $q_{\rm TIR}$ thus stems from errors on $L_{\rm TIR}$.

2.2. Distances and Source Classification

Optical data and photometric redshifts[13] are taken from the catalog of Ilbert et al. (2009). The wavelength range spanned by these observations (30 broad, medium, and narrowband filters) extends from 1550 Å to 8 μm. Capak et al. (2007, 2008) provide a complete description of these observations. Spectroscopic redshifts from the zCOSMOS survey (Lilly et al. 2009) or Magellan/IMACS and Keck/Deimos follow-up observations (e.g., Trump et al. 2009; J. S. Kartaltepe et al. 2010, in preparation) are available for ∼25% of our sources, most of which lie at $z \lesssim 1$. (See values of $f_{\rm spectro}(z)$, the spectroscopically observed sample fraction, in Figure 2.) The quality of distance measurements is assessed using spectroscopic confidence flags or the width of the photo-z probability distribution in the case of photometric redshifts (see S10, Appendix). Sources that do not fulfill the reliability requirements are excluded from the subsequent analysis. The optical photometry and spectroscopy were matched to the radio and IR catalog entries using a search radius of 0.″6 and 1″ (reflecting the larger uncertainty on the centroids of IR sources), respectively. As done for the band-merging of the *Spitzer* and VLA data, ambiguous optical-IR/radio associations are discarded.

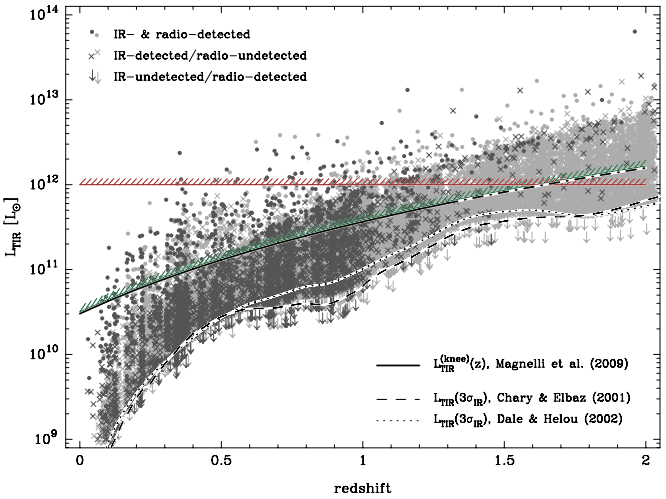

Figure 1. Infrared luminosities $L_{\rm TIR}$ of our 24 μm and/or 1.4 GHz detected sources (see the legend in the upper left corner) as a function of redshift. The dotted/dashed line tracing the lower edge of the measurements marks the minimal detectable $L_{\rm TIR}$ as predicted (based on 24 μm sensitivity) by template SEDs. Dark (light) gray symbols denote sources with spectroscopic (photometric) redshifts. The solid black line shows the evolution of the characteristic luminosity $L_{\rm TIR}^{\rm (knee)}$ of the TIR LF at $z < 1.3$ (Magnelli et al. 2009). Its extrapolation to $z \sim 2$ is schematically indicated by the dash-dotted segment. Red and green lines delimit the luminosity range of the two samples defined in Section 2.2.

In Figure 1, we plot the IR luminosities of our sources as a function of their redshift. Based on the range of accessible IR luminosities at each redshift we define two populations for later investigation: (1) ULIRGs with $L_{\rm TIR} \geqslant 10^{12}\ L_\odot$ and (2) all objects populating the bright end of the TIR luminosity function (LF) derived by Magnelli et al. (2009). The bright end is defined as $L_{\rm TIR} \geqslant L_{\rm TIR}^{\rm (knee)}(z)$, where $L_{\rm TIR}^{\rm (knee)}(z) \propto (1+z)^{3.6\pm0.4}$ represents the break in a double power-law parameterization[14] for the TIR LFs. Both selection approaches lead to a volume-limited sample of either ULIRGs or "IR-bright" galaxies spanning the range $z \lesssim 2$.

We divide our sample into SF galaxies and active galactic nuclei (AGNs) using a modification of the rest-frame optical color-based method developed by Smolčić et al. (2008). Optical-to-near-IR SED fits with the package ZEBRA (Feldmann et al. 2006) provide rest-frame $(u-K)$ colors that are translated into the probability of "SF-hood," Pr (SF), for each object in our sample (see Section 3 in S10). SF systems are all galaxies with Pr (SF) > 0.5 (or $(u-K)_{\rm AB} < 2.36$). Galaxies with redder colors are regarded as AGN hosts.

3. RESULTS

To constrain the evolution of average IR/radio ratios, we compute the median, $\langle q_{\rm TIR}\rangle$, in different redshift slices. The

[13] The photo-z dispersion $\sigma(\Delta z/(1+z))$ is 0.007, 0.013, and 0.051 for sources at $z < 1.25$ with $i_{\rm AB} < 22.5$, $i_{\rm AB} \in [22.5,\ 24]$, and $i_{\rm AB} > 24$, respectively. At higher redshifts, the accuracy of the photometric redshifts decreases by a factor of ∼3.

[14] Consistent with the measurement of Magnelli et al. (2009), Le Floc'h et al. (2005), and Caputi et al. (2007) report an evolution of $(1+z)^{3.2^{+0.7}_{-0.2}}$ and $(1+z)^{3.5\pm0.4}$, respectively, based on a *double exponential* fit to the TIR LF at $z \lesssim 1$.

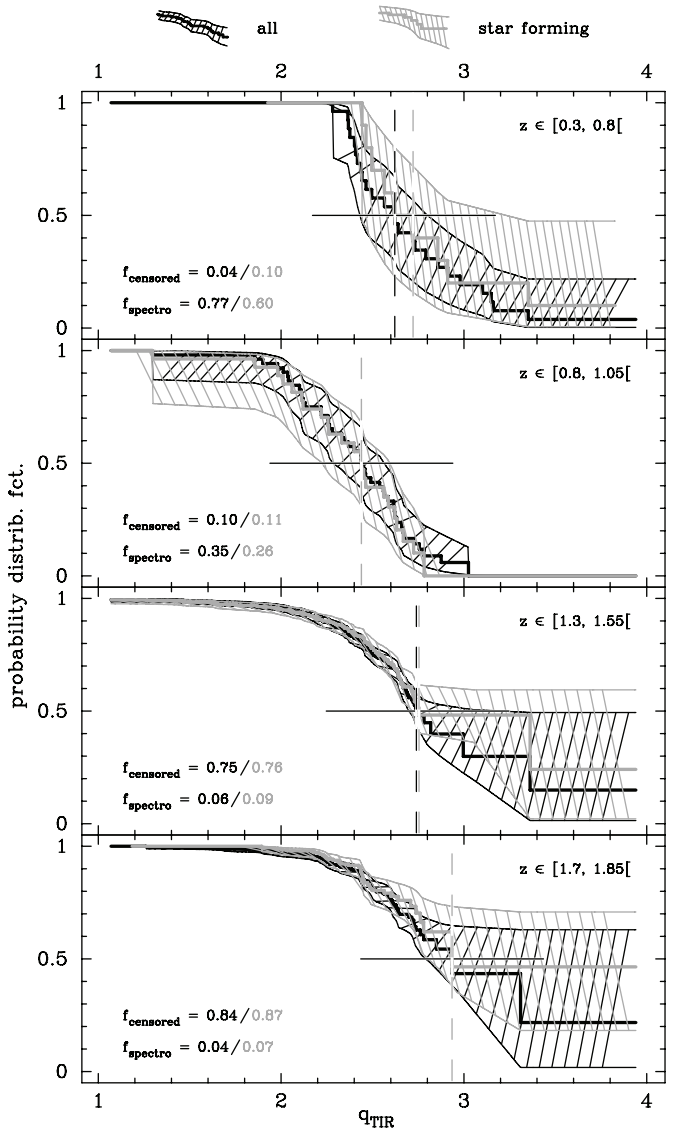

Figure 2. Cumulative distribution functions (CDFs) of ULIRG TIR/radio ratios, specifying the fraction of the population with a $q_{\rm TIR}$ larger than a given value on the horizontal axis. The panels show every second redshift bin from Figure 4. Hatched areas: 95% confidence interval. Gray: CDFs of SF objects. Black: all active galaxies. The intersection of the curves with the solid horizontal line defines the median $\langle q_{\rm TIR}\rangle$ (vertical dashed lines). $f_{\rm spectro}$ specifies the sample fraction with spectroscopically measured redshifts; $f_{\rm censored}$ is the fraction for which $q_{\rm TIR}$ is constrained by a lower limit.

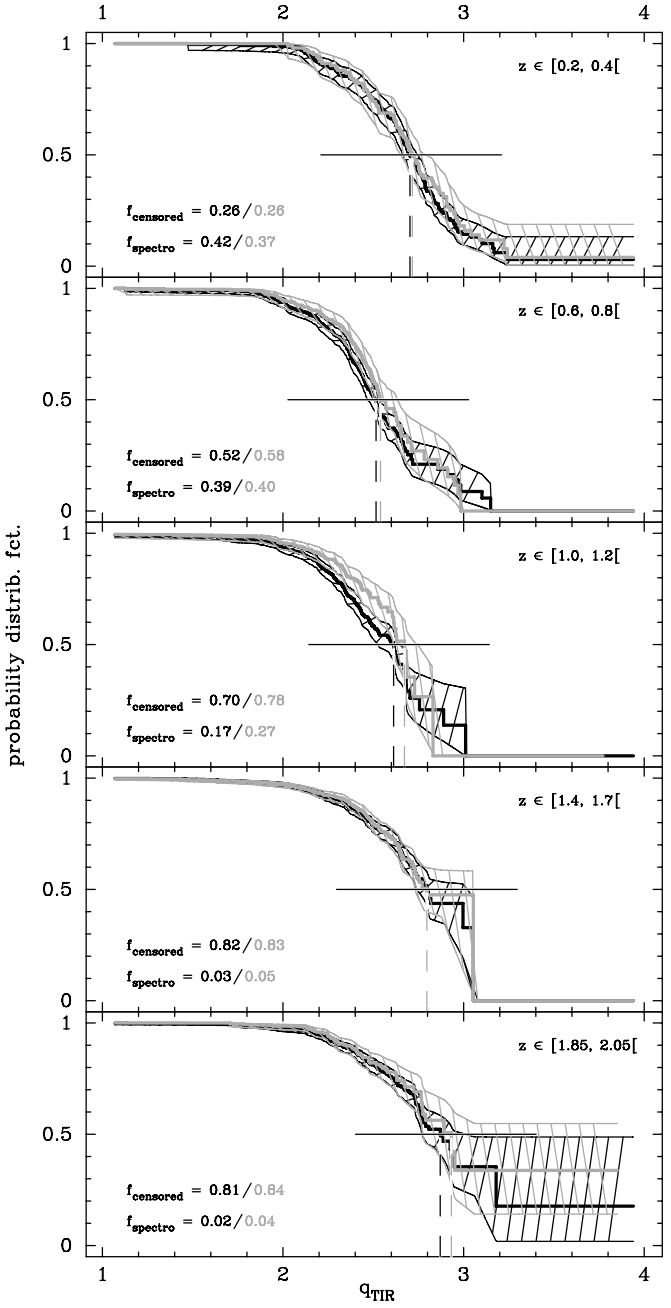

Figure 3. Same as Figure 2, but for the IR-bright population.

selection threshold for ULIRGs and the IR-bright population lies well above the faintest accessible IR luminosities in the redshift range $0 < z < 2$ (see Figure 1). Our samples are a mixture of (1) sources directly detected at IR *and* radio wavelengths, plus (2) 24 μm-detected sources with only a 3σ upper radio flux limit from the 1.4 GHz rms image. The corresponding IR/radio ratios are either well defined (within experimental uncertainties) or lower limits and, when combined, form a "censored" sample that is best analyzed with the tools of survival analysis. In the present case of one-sided censoring, the cumulative distribution function (CDF) of measurements of $q_{\rm TIR}$ can be derived with the Kaplan & Meier (1958) product limit estimator. As it is normalized (i.e., runs from zero to unity), the median corresponds to that $q_{\rm TIR}$ for which the CDF is equal to 0.5.

We derive $\langle q_{\rm TIR}\rangle$ for our sample of 1,692 SF ULIRGs and for all 3132 COSMOS ULIRGs (SF and AGN). Figure 2 shows the accordingly normalized CDFs. At $q_{\rm TIR} \gg \langle q_{\rm TIR}\rangle$, the CDFs approach a non-zero value reflecting the number of lower limits on $q_{\rm TIR}$ that may exceed the largest uncensored measurement in that bin. Due to the comparatively shallow VLA observations, IR sources without a directly detected 1.4 GHz counterpart become more frequent as redshift increases. Therefore, the width of the redshift bins chosen for the construction of the CDFs compromises between a split of the studied redshift range $z < 2$ into regular intervals and the aim to sample the distribution function down to the median. In Figure 3, we show the CDFs for IR-bright COSMOS sources (3004/5657 in the SF/total sample, respectively) that satisfy $L_{\rm TIR} \geqslant L_{\rm TIR}^{\rm (knee)}(z)$. The larger number of faint(er) luminosity sources allowed us to divide the range $z \lesssim 1.6$ into thinner slices than was done for ULIRGs. Moreover, there were a sufficiently large number of objects of this class even at low redshift ($0 < z < 0.2$), whereas the closest ULIRG in our sample lies at $z \sim 0.4$ (see Figure 1).

Table 1
Medians of the CDFs Shown in Figure 2

Sample/Galaxy Type	$\langle z \rangle$	$\langle q_{\rm TIR} \rangle$	N	$\langle z \rangle$	$\langle q_{\rm TIR} \rangle$	N
	ULIRG Sample			"IR-bright" Sample		
Local (all sources)	$0.099^{+0.020}_{-0.004}$	$2.674^{+0.020}_{-0.079}$	51	0.022 ± 0.001	$2.621^{+0.016}_{-0.013}$	1109
COSMOS				0.169 ± 0.014	$2.528^{+0.054}_{-0.061}$	34
(all sources)				0.346 ± 0.008	$2.703^{+0.041}_{-0.040}$	231
				0.518 ± 0.008	$2.629^{+0.067}_{-0.079}$	272
	0.659 ± 0.053	$2.622^{+0.179}_{-0.190}$	26	0.705 ± 0.004	$2.515^{+0.017}_{-0.047}$	486
				0.906 ± 0.005	$2.552^{+0.053}_{-0.034}$	754
	0.943 ± 0.022	$2.439^{+0.124}_{-0.154}$	52	1.108 ± 0.006	$2.612^{+0.034}_{-0.086}$	637
	1.200 ± 0.009	$2.548^{+0.083}_{-0.070}$	213	1.280 ± 0.007	$2.619^{+0.170}_{-0.056}$	487
	1.466 ± 0.004	$2.520^{+\infty}_{-0.042}$ (2.740)	715	1.498 ± 0.005	$2.576^{+0.239}_{-0.056}$ (2.796)	1506
	1.628 ± 0.003	$2.585^{+0.245}_{-0.057}$ (2.805)	553			
	1.785 ± 0.004	$2.715^{+\infty}_{-0.144}$ (2.935)	627	1.784 ± 0.004	$2.715^{+\infty}_{-0.146}$ (2.935)	546
	1.981 ± 0.003	$2.651^{+0.105}_{-0.104}$ (2.871)	1185	1.980 ± 0.003	$2.651^{+0.140}_{-0.102}$ (2.871)	875
Local (SF sources)	$0.095^{+0.015}_{-0.006}$	$2.703^{+0.055}_{-0.050}$	47	0.022 ± 0.001	$2.622^{+0.017}_{-0.012}$	1101
COSMOS				0.169 ± 0.015	$2.538^{+0.141}_{-0.115}$	19
(SF sources)				0.340 ± 0.014	$2.716^{+0.075}_{-0.064}$	101
				0.528 ± 0.010	$2.649^{+0.086}_{-0.117}$	142
	0.624 ± 0.062	$2.722^{+0.349}_{-0.279}$	10	0.705 ± 0.006	$2.540^{+0.092}_{-0.035}$	242
	0.940 ± 0.030	$2.439^{+0.156}_{-0.212}$	27	0.915 ± 0.007	$2.560^{+0.053}_{-0.037}$	394
				1.107 ± 0.008	$2.672^{+0.069}_{-0.061}$	327
	1.210 ± 0.012	$2.617^{+0.132}_{-0.082}$	119	1.273 ± 0.009	$2.709^{+\infty}_{-0.147}$	263
	1.467 ± 0.004	$2.534^{+\infty}_{-0.038}$ (2.754)	412	1.501 ± 0.006	$2.584^{+0.258}_{-0.066}$ (2.576)	932
	1.628 ± 0.004	$2.576^{+0.254}_{-0.080}$ (2.796)	348			
	1.786 ± 0.006	$2.715^{+\infty}_{-0.131}$ (2.935)	321	1.786 ± 0.006	$2.715^{+\infty}_{-0.132}$ (2.935)	268
	1.984 ± 0.004	$2.672^{+\infty}_{-0.121}$ (2.892)	591	1.982 ± 0.005	$2.712^{+\infty}_{-0.160}$ (2.932)	403

Notes. Bracketed values of $\langle q_{\rm TIR} \rangle$ are the medians in high-redshift bins before correction according to Equation (4).Column (1) sample description ; Columns (2) and (5) median redshift (with 1σ error) of redshift slice in which CDF is constructed; Columns (3) and (6) median TIR/radio ratio with upper and lower 95% confidence intervals; Columns (4) and (7) the numbers of objects used.

The values of $\langle q_{\rm TIR} \rangle$ reported in Table 1 increase at $z \gg 1$. In S10 (Figure 17 and Table 6) we found that—although average IR/radio ratios display little evolution with redshift—the dispersion $\sigma_{q_{\rm TIR}}$ in the COSMOS data increases fairly abruptly at $z \sim 1.4$. This is primarily due to increased uncertainties in $q_{\rm TIR}$, but might also hide a small intrinsic increase in the dispersion. The scatter $\sigma_{q_{\rm TIR}}$ directly influences the shift (e.g., Kellermann 1964)

$$\Delta q_{\rm bias} = \ln(10)\,(\beta - 1)\,\sigma^2_{q_{\rm TIR}} \quad (3)$$

between the average IR/radio ratio of flux-limited samples selected at IR and radio wavelengths (β is the power-law index of the differential source counts $dN/dS \propto S^{-\beta}$). S10 showed that Equation (3) predicts the actual offsets present in the COSMOS data remarkably well. Because of the higher sensitivity of the 24 μm observations, the present sample is effectively IR-selected. Equation (3) allows us to compensate for the relative offset between medians at high and low redshift that arises *artificially* due to the increased scatter in our data at $z \gtrsim 1.4$. In doing so, we (1) use that $\overline{\sigma}_{q_{\rm TIR}}(z \lesssim 1.4) \approx 0.35$ and $\overline{\sigma}_{q_{\rm TIR}}(1.4 \lesssim z < 2) \approx 0.75$ (see S10, Table 6), and we (2) assume that the observed flux densities of galaxies at $z > 1.4$ primarily lie in a range of sub-Euclidean source counts where $\beta \approx 1.5$ (e.g., Chary et al. 2004; Papovich et al. 2004). The resulting correction (to be subtracted from the medians at $z > 1.4$) is

$$\begin{aligned} {\rm D}q_{\rm corr} &= \Delta q_{\rm bias}(1.4 \lesssim z < 2) - \Delta q_{\rm bias}(z < 1.4) \\ &= \ln(10)[(1.5\text{–}1) \times 0.75^2 - (2.5\text{–}1) \times 0.35^2] \simeq 0.22, \end{aligned} \quad (4)$$

with an associated uncertainty (owing to the errors on $\overline{\sigma}_{q_{\rm TIR}}$ and β) of approximately 0.13. Our step function-like correction neglects that sources at a given redshift may be drawn from a flux range with continuously varying β. This is the simplest possible form that allows us to correctly compensate for an apparent, spurious offset in $\langle q_{\rm TIR} \rangle$ between the limits of our investigated redshift range.

In Figure 4, we plot $\langle q_{\rm TIR} \rangle$ versus redshift and relate these medians with the best-fitting evolutionary trend of the form $\langle q_{\rm TIR}(z) \rangle / \langle q_{\rm TIR}(z = 0) \rangle \propto (1+z)^{\gamma}$ for each of our (sub)samples. To constrain the fit at low redshift, we add a low-z data point (both for the ULIRG and the IR-bright sample) based on the complete *IRAS*-selected sample of Yun et al. (2001). The values of $q_{\rm FIR}$ given by Yun et al. (2001) were converted[15] to $q_{\rm TIR}$ by boosting their IR flux by a factor of 2, the average difference between the mean $q_{\rm TIR}$ and $q_{\rm FIR}$ found by Bell (2003). Since SF

[15] Due to the well-constrained mean IR/radio ratios in the samples of Yun et al. (2001) ($\langle q_{\rm FIR} \rangle = 2.34 \pm 0.01$) and Bell (2003) ($\langle q_{\rm TIR} \rangle = 2.64 \pm 0.02$) this *average* correction factor is accurate to within a few percent.

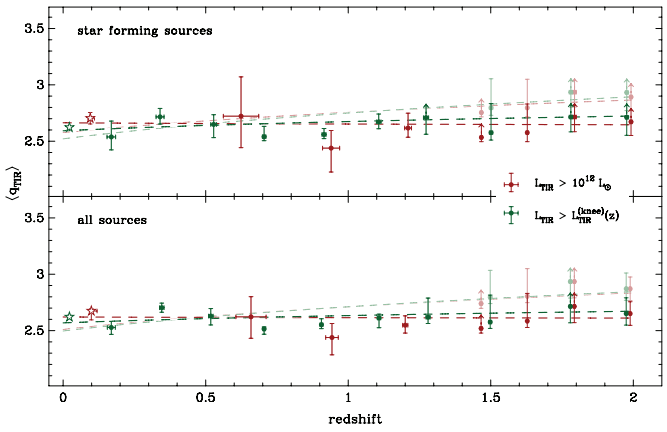

Figure 4. Redshift evolution of the median logarithmic TIR/radio ratio $\langle q_{\rm TIR}\rangle$ for IR-bright galaxies ($L_{\rm TIR} > L_{\rm TIR}^{\rm (knee)}$; green symbols) and ULIRGs (red). In the upper panel, we consider the subset of SF sources, extracted from the entire sample of active galaxies (bottom). Transparent symbols: estimates of $\langle q_{\rm TIR}\rangle$ prior to correction for selection biases (see Section 3). The best-fitting evolutionary trends to the corrected (uncorrected) measurements of $\langle q_{\rm TIR}\rangle$ are reported using strong (transparent) dashed lines. They have been additionally constrained (open stars) at low redshift by the sample of Yun et al. (2001). Both ULIRGs and IR-bright galaxies have constant average IR/radio properties out to $z \sim 2$ when correcting for bias, otherwise ∼0.3 dex of positive evolution is found.

systems in the sample of Yun et al. (2001) could not be identified following the procedure employed for the COSMOS galaxies (see Section 2.2), our reference sample for SF galaxies simply consists of all local sources with $L_{1.4\,\rm GHz} < 10^{24}$ W Hz^{-1}, in keeping with Condon (1989).

The two panels of Figure 4 show the evolutionary trends for SF systems (top) and all galaxies (SF and AGN; bottom). To account for the asymmetric error bars, we have drawn 1001 values from within the 95% confidence region of each median[16] and then fit the evolutionary trend 1001 times based on random combinations (without replacement) of the resampled medians. The final best-fit values given below are the medians of the parameter distributions thus obtained.

If the uncorrected high-z medians are included in the evolutionary fit, we find an exponent $\gamma = 0.09^{+0.08}_{-0.07}/0.11^{+0.06}_{-0.05}$ for ULIRGs (SF and total sample, respectively) and $\gamma = 0.13 \pm 0.06/0.12 \pm 0.04$ for the IR-bright galaxies. (Errors delimit the 95% confidence interval.) This would imply a doubling of the average TIR/radio flux ratio from redshift 0 to 2, with most of the evolution happening at $z \gtrsim 1.4$. By taking the corrected medians at $z \gtrsim 1.4$ into consideration, we find an evolution of the average IR/radio ratios of ULIRGs according to $(1+z)^{-0.01\pm0.06}$ (identical for SF and all ULIRGs). Similarly, the trend for the IR-bright population is consistent with being zero, both for the total sample ($\gamma = 0.03^{+0.05}_{-0.04}$) and the SF subset where $\gamma = 0.04^{+0.06}_{-0.05}$.

4. CONCLUSIONS

We have presented the first investigation of the evolution of the IR–radio relation out to $z \sim 2$ for a statistically significant, volume-limited sample of IR-luminous galaxies. This advance became possible thanks to two factors: (1) the large area and deep mid-IR coverage of the COSMOS field, and (2) the inclusion of flux limits in the analysis with appropriate statistical tools.

[16] When upper confidence limits are ∞, we set the upper error bar to twice the lower one. This eases the calculation of γ, while reflecting that upper and lower confidence intervals are generally similar down to the 60 percentile of the CDF.

At redshifts $z < 2$, the median TIR/radio ratio of ULIRGs remains unchanged if we compensate for biases. On the most basic level, this implies that their magnetic fields, B, are sufficiently strong to ensure that cosmic-ray electrons predominantly lose their energy through synchrotron radiation (rather than inverse Compton scattering off the CMB). Regarding the 0.3 dex increase of the uncorrected evolutionary signal as an upper limit implies that $B \gtrsim 30\ \mu$G (e.g., Murphy 2009, Figure 5), as expected for compact and strong starbursts. This conclusion applies to both SF systems and optically selected AGN hosts, consistent with the similar mean IR/radio ratios reported for these two classes of objects in S10. Our finding agrees with theoretical and numerical expectations that ULIRGs should follow the local IR–radio relation until at least $z \sim 2$ (Lacki & Thompson 2010; Murphy 2009). Moreover, it suggests that the lower IR/radio ratios frequently reported for high-z SMGs (e.g., Kovács et al. 2006; Valiante et al. 2007; Murphy et al. 2009; Michałowski et al. 2010; but see also Hainline et al. 2009) are not typical of distant ULIRGs in general.

Our complete sample of "IR-bright" galaxies—the population that resides on the evolving bright end of the TIR LF—links high-z ULIRGs to normal IR-galaxies ($\log(L_{\rm TIR}/L_\odot) \gtrsim 10.5$) in the local universe. The fact that the average IR/radio ratio of the latter is very similar to that of ULIRGs demonstrates that the similar IR/radio properties of existing SF samples at low and high redshift are not the fortuitous consequence of comparing objects in different luminosity ranges. While distant starbursts follow the same IR–radio relation as local sources, this has not yet been ascertained for galaxies with moderate SF rates ($\lesssim 10\,M_\odot$ yr^{-1}) that cannot be directly detected with current radio and far-IR facilities. The recent stacking analyses of Seymour et al. (2009) and Ivison et al. (2010) measured a steady decline of average IR/radio ratios that begins at $z < 1$ and continues out to $z > 2$. Given that the average IR luminosities of their image stacks are comparable to those of our "IR-bright" sample these findings are at odds with our measurements and, as shown here, cannot be ascribed to a luminosity offset between low and high redshift sources. It is to be expected that the origin of the discrepancy—possibly the different methodology, sample selection, or SED evolution (e.g., Symeonidis et al. 2009; Seymour et al. 2010)—will soon be identified in upcoming EVLA and Herschel surveys by virtue of the increased sensitivity and/or wavelength coverage these observatories offer. The latter capability in particular will ensure more accurate measurements of radio spectral indices and a better sampling of dust emission well into the far-IR which is crucial to the determination of the dust temperatures in distant starbursts. These improvements should also lead to a decrease in the scatter of the IR–radio relation at high redshift, thereby reducing both the need for and the impact of bias corrections of the kind that were applied in this work.

M.T.S. acknowledges DFG-funding (grant SCHI 536/3-2) and thanks Gianni Zamorani and Rob Ivison for reading and commenting on the manuscript.

This work is partly based on observations made with the *Spitzer Space Telescope*, which is operated by NASA/JPL/Caltech. The National Radio Astronomy Observatory (NRAO) is operated by Associated Universities, Inc., under cooperative agreement with the National Science Foundation.

Facilities: VLA, *Spitzer* (IRAC, MIPS), VLT:Melipal, Subaru (SuprimeCam)

REFERENCES

Appleton, P. N., et al. 2004, ApJS, 154, 147
Bell, E. F. 2003, ApJ, 586, 794
Capak, P., et al. 2007, ApJS, 172, 99
Capak, P., et al. 2008, VizieR Online Data Catalog, 2284, 0
Caputi, K. I., et al. 2007, ApJ, 660, 97
Carilli, C. L., et al. 2008, ApJ, 689, 883
Chary, R., & Elbaz, D. 2001, ApJ, 556, 562
Chary, R., et al. 2004, ApJS, 154, 80
Condon, J. J. 1989, ApJ, 338, 13
Condon, J. J. 1992, ARA&A, 30, 575
Dale, D. A., & Helou, G. 2002, ApJ, 576, 159
Dunkley, J., et al. 2009, ApJS, 180, 306
Feldmann, R., et al. 2006, MNRAS, 372, 565
Frayer, D. T., et al. 2006, AJ, 131, 250
Frayer, D. T., et al. 2009, AJ, 138, 1261
Garn, T., Green, D. A., Riley, J. M., & Alexander, P. 2009, MNRAS, 397, 1101
Garrett, M. A. 2002, A&A, 384, L19
Hainline, L. J., Blain, A. W., Smail, I., Frayer, D. T., Chapman, S. C., Ivison, R. J., & Alexander, D. M. 2009, ApJ, 699, 1610
Helou, G., Soifer, B. T., & Rowan-Robinson, M. 1985, ApJ, 298, L7
Ibar, E., Ivison, R. J., Biggs, A. D., Lal, D. V., Best, P. N., & Green, D. A. 2009, MNRAS, 397, 281
Ibar, E., et al. 2008, MNRAS, 386, 953
Ilbert, O., et al. 2009, ApJ, 690, 1236
Ivison, R. J., et al. 2010, MNRAS, 402, 245
Kaplan, E. L., & Meier, P. 1958, J. Am. Stat. Assoc., 53, 457
Kartaltepe, J. S., et al. 2010, ApJ, 709, 572
Kellermann, K. I. 1964, ApJ, 140, 969
Kovács, A., Chapman, S. C., Dowell, C. D., Blain, A. W., Ivison, R. J., Smail, I., & Phillips, T. G. 2006, ApJ, 650, 592
Lacki, B. C., & Thompson, T. A. 2010, ApJ, submitted (arXiv:0910.0478)
Le Floc'h, E., et al. 2005, ApJ, 632, 169
Le Floc'h, E., et al. 2009, ApJ, 703, 222
Lilly, S. J., et al. 2009, ApJS, 184, 218
Magnelli, B., Elbaz, D., Chary, R. R., Dickinson, M., Le Borgne, D., Frayer, D. T., & Willmer, C. N. A. 2009, A&A, 496, 57
Michałowski, M. J., Hjorth, J., & Watson, D. 2010, A&A, in press (arXiv: 0905.4499)
Murphy, E. J. 2009, ApJ, 706, 482
Murphy, E. J., Chary, R.-R., Alexander, D. M., Dickinson, M., Magnelli, B., Morrison, G., Pope, A., & Teplitz, H. I. 2009, ApJ, 698, 1380
Papovich, C., et al. 2004, ApJS, 154, 70
Sanders, D. B., et al. 2007, ApJS, 172, 86
Sargent, M. T., et al. 2010, ApJS, 186, 341 (S10)
Schinnerer, E., et al. 2007, ApJS, 172, 46
Schinnerer, E., et al. 2010, ApJS, submitted
Seymour, N., Huynh, M., Dwelly, T., Symeonidis, M., Hopkins, A., McHardy, I. M., Page, M. J., & Rieke, G. 2009, MNRAS, 398, 1573
Seymour, N., Symeonidis, M., Page, M. J., Huynh, M., Dwelly, T., McHardy, I. M., & Rieke, G. 2010, MNRAS, 402, 2666
Smolčić, V., et al. 2008, ApJS, 177, 14
Symeonidis, M., Page, M. J., Seymour, N., Dwelly, T., Coppin, K., McHardy, I., Rieke, G. H., & Huynh, M. 2009, MNRAS, 397, 1728
Trump, J. R., et al. 2009, ApJ, 696, 1195
Valiante, E., Lutz, D., Sturm, E., Genzel, R., Tacconi, L. J., Lehnert, M. D., & Baker, A. J. 2007, ApJ, 660, 1060
Yun, M. S., Reddy, N. A., & Condon, J. J. 2001, ApJ, 554, 80